Dust model sensitivity to dust source mask, sandblasting efficiency, air density, and land use: Implications for model improvement

Janak R. Joshi

George Mason University, Fairfax, VA 22030, USA

NASA Goddard Space Flight Center, Greenbelt, MD 20771, USA

University of Maryland Baltimore County, Baltimore, MD 21250, USA

Abstract

This study compares dust storm simulations using two commonly adopted methods for representing four important dust emission parameters. Compared to a dynamic dust source mask based on land use and vegetation cover, a static mask based solely on land use overestimates dust concentration and optical depth by a factor of 2, besides generating spurious emissions. The results reinforce that seasonal variations in vegetation cover can significantly affect dust emissions. For sandblasting efficiency, a clay-dependent semiempirical expression produces 10 times more dust than a physics-based expression. Simulations using model-predicted versus a fixed constant for air density differ by only 8%. However, this difference could range between 12 and 22% for annual simulations over global dust source regions. Simulations with updated versus old land use data, using the same dust source mask, differ twofold, indicating the significant impact of land use change on regional dust emission in central Arizona. The differences in the pairs of these simulations are generally larger than the uncertainty due to meteorology. The simulations align better with observation when using the dynamic dust source mask, the physics-based sandblasting efficiency, and the up-to-date land use data. Given the high sensitivity of dust to surface conditions, the results discussed have implications for improving the dust cycle in weather and climate models and for interpreting model intercomparisons.

Keywords:
Dust-emission sources; Vegetation; Land use change; Clay; Ensemble simulation

1. Introduction

Physics-based models are essential for understanding the atmospheric dust cycle and its interactions with climate, air quality, and the environment. These models can help mitigate the costly adverse impacts of dust and dust storms on public health and property. Consequently, numerous field, laboratory, computational, and theoretical studies have been carried out to understand the dust emission process and develop predictive models (Bagnold, 1941; White, 1979; d'Almeida, 1987; Gillette and Passi, 1988; Tegen and Fung, 1994; Marticorena and Bergametti, 1995; Shao et al., 1996; Fécan et al., 1999; Alfaro and Gomes, 2001; Ginoux et al., 2001; Prospero et al., 2002; Kok et al., 2014). Despite satisfactory performance in many applications, these models exhibit significant uncertainties, an order of magnitude or higher (Todd et al., 2008; Huneeus et al., 2011; Wu et al., 2020). The discrepancy between models and observations depends on how well the models represent processes or parameters such as dust source areas, sediment availability, threshold friction velocity, size distribution and range, wet and dry deposition, point-scale to grid-scale upscaling of parameters amid sub-grid scale heterogeneities, and input data, including meteorology (Schulz et al., 1998;

*Corresponding author
Email address: jjoshi1@umbc.edu (Janak R. Joshi)

Shao, 2008; Kok, 2011; Webb and Strong, 2011). Challenges in accurately accounting for these processes and lacking data have prompted model simplifications. Intermodel disagreements arise from differences in dust emission schemes or their implementations, which dictate how the various processes or quantities (parameters) involved are represented (e.g., Darmenova et al., 2009; Kang et al., 2011; Menut et al., 2013). These include parameters such as wind erosion threshold velocity including corrections for drag-partition and soil-cohesion, sandblasting efficiency, dust source specification, particle size distribution (size range and the method, sectional versus modal), and various input data characterizing the surface (Raupach and Lu, 2004; Zender et al., 2003; Timmreck and Schulz, 2004; Menut et al., 2007; Shao et al., 2011; Joshi, 2021). Recently, satellite-derived albedo-based drag-partitioning was reported to improve dust simulations (e.g., LeGrand et al., 2023; Hennen et al., 2023), but the results could be subject to errors due to flaws in the albedo-based roughness parameters (approach of Chappell and Webb, 2016, cited in Okin (2023); see Okin (2023)). Additionally, intermodel disagreement can stem from variations in transport (including deposition) and meteorological components (Maring et al., 2003; Colarco et al., 2003; Grini and Zender, 2004; Uno et al., 2006; Nowottnick et al., 2011).

Focusing on the emission part of the models, this study examines the sensitivity of dust simulation to parameter representation in a dust emission scheme, in which threshold friction velocity is observationally constrained rather than parameterized. Such analysis could provide estimates for model uncertainty linked to these parameters, and provide insights to decide model configuration and to interpret model intercomparisons. The procedure involves generating a control or reference simulation, followed by generating sensitivity simulations by altering the representation for a specific parameter in the dust emission scheme (dust emission model). The study tests two different methods, both commonly known in the literature, for representing the four parameters: dust source mask, sandblasting efficiency, air density, and land use. These parameters generally appear as a multiplier in a dust flux equation or influence the threshold velocity for wind erosion (e.g., Eq. (1)). Consequently, these can significantly impact patterns and magnitudes of dust emission and concentration. The study also compares the parameter sensitivities with the sensitivity due to meteorology alone. Such studies appear to be relatively scarce, especially within the presented context—detailed analysis at high resolution, evaluations for both dust concentration and optical depth, ensemble simulations, and comparison with sensitivity (uncertainty) due to meteorology in a consistent modeling framework.

The reference simulation utilized the same configuration for the dust emission model as in Joshi (2021) (hereafter J21), which successfully simulated the tested dust storm. J21 employed a single configuration for the dust emission model parameters, determined through a literature survey and physical reasoning, with a primary focus on agreement with observations. In contrast, the present study conducted additional (sensitivity) simulations by modifying the configuration from the reference to address the question: how would the simulations differ if an alternative dust emission parameter representation was employed? The reference simulation differed from J21 solely in meteorology, turning off nudging and utilizing an ensemble of simulations rather than a single realization. Section 2 describes the materials and methods, followed by Section 3 presenting the results and discussions, and Section 4 ending the paper with conclusions.

2. Methods and data

2.1 Model configuration

The same dust modeling system—comprising the Weather Research and Forecasting (WRF), FENGSHA (a dust emission model), and Community Multiscale Air Quality (CMAQ) models—and configuration, including the same 1 km horizontal resolution and the same initial and boundary conditions as used in Joshi (2021) or J21, except turning off the meteorological nudging, was employed to generate the reference simulation for the same case of 8–9 April 2013 Arizona dust storm caused by a cold front. (More details about this dust storm, including the synoptic developments, can be found in Sect. 2.3.2 of Joshi (2023).) The nudging was disabled unless stated explicitly to ensure no contribution of meteorology toward any difference between dust simulations (i.e., the difference between dust simulations differing only in dust emission parameter representation). The WRF model was initialized every third hour on 6 April 2013, producing eight different realizations for meteorology, each saved at a 15-minute frequency. Corresponding to these realizations, an 8-member ensemble dust simulation was generated with the chemical transport model CMAQ (with dust emissions computed offline) initialized at 0 UTC on 8 April 2013 and for the following two days. The ensemble simulations were carried out for the sake of statistical significance.

First, the reference or control simulation ControlE was generated as discussed above. Then, four sensitivity experiments were carried out by changing from the control, one at a time, the representation for each of the four parameters—dust source mask, sandblasting efficiency, air density, and land use. The details on these parameters and the dust emission model are provided in Sect. 2.1.1. Finally, dust simulation—quantified in terms of the surface-concentration of particulate matter with a diameter less than 10 μm (PM_{10}) and column abundance of dust (or dustiness) represented by dust optical depth (DOD)—from each sensitivity experiment was compared with ControlE. The modeled DOD was calculated by subtracting from the total aerosol optical depth (AOD) the AOD portion attributable to non-dust-related emissions (AOD from a no-dust experiment that excluded dust emissions).

2.1.1. Dust emission model

Saltation bombardment or sandblasting is assumed to be the dust emission mechanism. The horizontal flux of saltating sand particles is multiplied by saltation bombardment efficiency (Shao et al., 1993) or sandblasting efficiency to calculate the vertical flux F ($\mathrm{g\,m^{-2}s^{-1}}$) of dust particles (Owen, 1964; Raupach and Lu, 2004):

$$\begin{aligned} \mathrm{F} &= \frac{C\rho_a}{g}\sum_{l=1}^{L}\sum_{s=1}^{S} K_{vh} M_l A_l E_s \times u_*(u_*^2 - u_{*t,ls}^2), \text{ if } u_* > u_{*t,ls} \\ &= 0, \text{ otherwise.} \end{aligned} \tag{1}$$

where C is a dimensionless constant, g is the acceleration of gravity, u_* is wind friction velocity, $u_{*t,ls}$ is the threshold friction velocity for the erodible land type l and soil type s, E_s is the soil wind erodibility, and K_{vh} is the sandblasting efficiency. The M_l and A_l denote the dust source mask and the fraction of the wind-erodible land type (the surface from which sediment deflation can occur), respectively. The ρ_a is the surface air density. Together, the product $M_l \times A_l \times E_s$ can be viewed as an 'erodibility' parameter. More details on this dust emission model can be found in J21.

2.2 Experimental details

2.2.1. Dust source mask

A dust source mask (M_l in Eq. (1)) identifies and assigns dust emission strength to wind-erodible areas based on surface characteristics. As such, it is one of the key parameters affecting dust production. Two methods for creating the dust source mask are tested. The first method considers both land use and near real-time vegetation cover. The dust-suppression effect of vegetation is represented using the satellite-derived 250-m resolution NDVI (Normalized Difference Vegetation Index based on the MODIS data, see J21). For desert land types, the mask value is 1.0 if NDVI is less than 0.1, and it decreases linearly from 0.7 to 0.3 as NDVI increases from 0.10 to 0.13. For cropland, the mask equals 1.0 for pixels with NDVI below 0.25. This dynamic mask, which has also been used in previous studies (see J21), was used in the control (reference) experiment ControlE. The second method is simpler and considers only land use. In this method, the mask values of 0.5, 0.25, 0.75, and 0.75 are assigned to shrubland, shrubgrass, sparse-barren land, and cropland, respectively (Fu et al., 2014). This time-static (or simply static) mask was used in the sensitivity experiment referred to as StatMask.

2.2.2. Sandblasting efficiency

The vertical flux of the emitted dust is typically computed by multiplying the horizontal saltation flux with sandblasting efficiency (K_{vh} in Eq. (1)), which represents the soil's ability to release suspendable particles. Therefore, K_{vh} is one of the key factors determining the amount of the emitted dust aerosol. Lu and Shao (1999) developed a parameterization for K_{vh} by considering the removal of dust from a small crater formed by the impact of a saltator particle plowing through the soil surface. Solving particle motion equations with some simplifications, they obtained an expression, consistent with field measurements (Lu and Shao, 1999):

$$K_{vh} = \frac{C_\alpha g f \rho_b}{2p}\left(0.24 + C_\beta u_* \sqrt{\frac{\rho_p}{p}}\right) \tag{2}$$

where p is the soil plastic pressure (a measure of surface hardness), f is the fraction of dust in the crater volume, ρ_p and ρ_b are the particle and bulk soil densities, respectively, and C_α and C_β are constants of order 1. All these parameters are soil-specific. This expression captures the dependence of dust emission on variable wind conditions, through friction velocity u_*, as well as on soil-surface hardness, among other soil properties. The expression has been adopted by many recent studies (e.g., Foroutan et al., 2017; Joshi, 2021). Other physics-based K_{vh} parameterizations can be found elsewhere (e.g., Alfaro and Gomes, 2001; Kok et al., 2014). Another parameterization that is tested here is purely empirical (Marticorena and Bergametti, 1995) (hereafter MB95), with some extrapolation (such as used in Dong et al., 2016; Fu et al., 2014):

$$\begin{aligned} K_{vh} &= 10^{13.4\times clay-6},\ \text{if } clay \leq 0.2 \\ &= 2\times 10^{-4},\ \text{if } clay > 0.2, \end{aligned} \tag{3}$$

where *clay* represents the surface-soil clay fraction. The first part of Eq. (3) is based on the work of MB95, who assumed that a soil's ability to release suspendable particles should be related to its clay content, because clay consists of the smallest soil particles. The second part according to Dong et al. (2016) is based on the recommendation of MB95. Due to the extrapolation part, the expression is referred to here as 'semiempirical.' The physics-based expression (Eq. (2), with parameters based on Kang et al. (2011)) was used in ControlE and the clay-based one (Eq. (3)) in the sensitivity experiment named ClayKvh.

2.2.3. Air density

The quantity of dust emitted is proportional to surface air density (ρ_a in Eq. (1)), due to the greater erosive power of denser air. Dust emission models often assume a fixed constant for air density, ~ 1.23 $\mathrm{kg\,m^{-3}}$ (e.g., Marticorena and Bergametti, 1995; Hennen et al., 2023), corresponding to the standard at sea level (Darmenova et al., 2009). However, spatial and periodic-temporal fluctuations in surface air density (caused by elevation differences, the diurnal cycle, or advection) can influence wind power (Liang et al., 2022) and therefore dust emission. Within the modeling domain of this study with complex topography, the model-predicted surface air density ranged from 0.91 to 1.16 $\mathrm{kg\,m^{-3}}$, differing by $\sim 27\%$ across space, and from 1.06 to 1.11 $\mathrm{kg\,m^{-3}}$, differing by $\sim 5\%$ across time (computed over a diurnal cycle spanning the dust storm, 12 UTC to 12 UTC). Model-predicted air density that varies dynamically was used in the control experiment, while a fixed constant $\sim 1.25\,\mathrm{kg\,m^{-3}}$ (value from the previous version of the model) was used in the sensitivity experiment referred to as FxdAdens.

2.2.4. Land use

Only certain land types such as barren, shrub, or cropland emit dust significantly, and some do more efficiently than others. For example, disturbed cropland emits more efficiently than undisturbed shrubland. The specification of land types can affect dust emission in the model through three terms: the dust source mask, the threshold friction velocity, and the fraction of the erodible land type (M_l, $u^*_{t,ls}$, and A_l in Eq. (1)). Two data sets for land use are tested. One is the Biogenic Emissions Landuse Database, Version 3 (BELD3) (Kinnee et al., 1997) data set (https://www.epa.gov/air-emissions-modeling/biogenic-emissions-landuse-database-version-3-beld3), a commonly used data set for the inline dust emission scheme in the community CMAQv5.3 (e.g., Huang and Foroutan, 2022). This data is time-invariant and includes information collected some 20 years earlier than the simulated dust storm. The other data set is up-to-date and was created (detail in J21) using the 30 m resolution Cropland Data Layer (CDL; Han et al. (2012)) from the US Department of Agriculture for the year 2013. The CDL-based up-to-date data was used in ControlE and the old BELD3 data in the sensitivity experiment referred to as Beld3Lnd. In the two experiments, the dust source mask M_l remains the same and any difference between the simulations will be only through the threshold friction velocity and erodibility ($u^*_{t,ls}$ and A_l).

2.3 Data and metrics

The following data sets are used: ground-based hourly observations of PM_{10} from the US Environmental Protection Agency's Air Quality System, satellite-derived dust optical depth (DOD; ∼10 km resolution) from the Aqua-MODIS Deep Blue aerosol product (Ginoux et al., 2012), and hourly METeorological Aerodrome Reports (METAR) station data from the NCEP's Meteorological Assimilation Data Ingest System. More details about these data including station locations can be found in J21. The spatial aggregates are computed across the same two regions defined in J21, away from the domain boundaries. One of these regions is urban or Phoenix (Phx), which is far from dust sources, and the other is rural or western Pinal County (WPnl), which is near dust sources. Both the regions are indicated in Fig. 3. Furthermore, global high-resolution (0.1° spatial) land data from the fifth generation of European ReAnalysis (Muñoz-Sabater, J. et al., 2021) or ERA5-Land are used to analyze the impact of air density variations across the Earth's potential dust source regions. The ERA5-Land includes hourly averages for all months of the year 2013, each month having 24 values, for the hours 00–23.

The metrics to compare model results with observations include the mean bias (MB), the normalized mean bias (NMB), the mean absolute error (MAE), and the index of agreement (IOA). These are defined as MB $= \sum_{i=1}^{n} \frac{m_i - o_i}{n}$, NMB $= \frac{\sum_{i=1}^{n} m_i - o_i}{\sum_{i=1}^{n} o_i} \times 100\,\%$, MAE $= \sum_{i=1}^{n} \frac{|m_i - o_i|}{n}$, and IOA $= 1 - \frac{\sum_{i=1}^{n}(m_i - o_i)^2}{\sum_{i=1}^{n}(|m_i - \bar{o}| + |o_i - \bar{o}|)^2}$; where n is the sample size, m_i and o_i are the i^{th} model and observation values, respectively, and $\bar{o}$ is the mean of the observations.

Similar quantities are used to compare sensitivity simulations with the control (ControlE). Corresponding to MB and MAE, the mean difference (MD) and the mean absolute difference (MAD) referring to a sensitivity experiment are calculated by replacing the observation (in 'model minus observation') with ControlE values. Whether a particular metric refers to calculations relative to the observation or to the control is indicated by the suffixes 2Obs or 2Ctl, respectively. Therefore, MB2Obs will denote the mean bias relative to the observation, MD2Ctl the mean difference relative to the control (model minus ControlE), IOA2Ctl the index of agreement relative to the control (i.e., observation in the IOA expression replaced by ControlE), and so on. Another metric is the ratio of means (RatM), as RatM2Obs, when the mean of model values is divided by that of observation, or as RatM2Ctl, when the division is by the mean of the control.

The statistical significance of the difference between simulations is determined using the Welch's t-test at a significance level (α) of 0.05.

3. Results and discussion

3.0.1. Meteorological simulations

Since dust emission and concentration are highly sensitive to surface wind, the simulated wind is compared against the observed one in Fig. 1, which shows time series for wind speed and direction with inset measures of model performance. The performance metrics include mean bias MB, mean absolute error MAE, root mean squared error RMSE, index of agreement IOA, and circular correlation coefficient ρ_{circ}. Overall, the wind speed is simulated well (e.g., MAE $< 1.54\,\mathrm{ms^{-1}}$, RMSE $< 2.28\,\mathrm{ms^{-1}}$, IOA ~ 0.9), although discrepancies can also be seen including for high wind speeds relevant to dust emission. The agreement with observation is lower than in J21 (which used nudging), and this bias may affect dust estimates. The simulated precipitation largely resembled J21 (Fig. 7 therein), with no precipitation around the domain center, the main dust-producing region (high dust-source-mask values in Fig. 4 in J21). However, a small precipitation band near the center of the domain was absent (for hours 00 and 01 over the top edge of the western Pinal County). This absence may contribute to dust biases. Challenges in accurately simulating meteorology for the complex-terrain studied region have also been noted earlier. Nevertheless, the obtained accuracy should suffice for the purpose of this study—to analyze dust emission parameter sensitivity. Moreover, the study estimates meteorology-induced dust uncertainty and discusses parameter sensitivity in relation to this uncertainty.

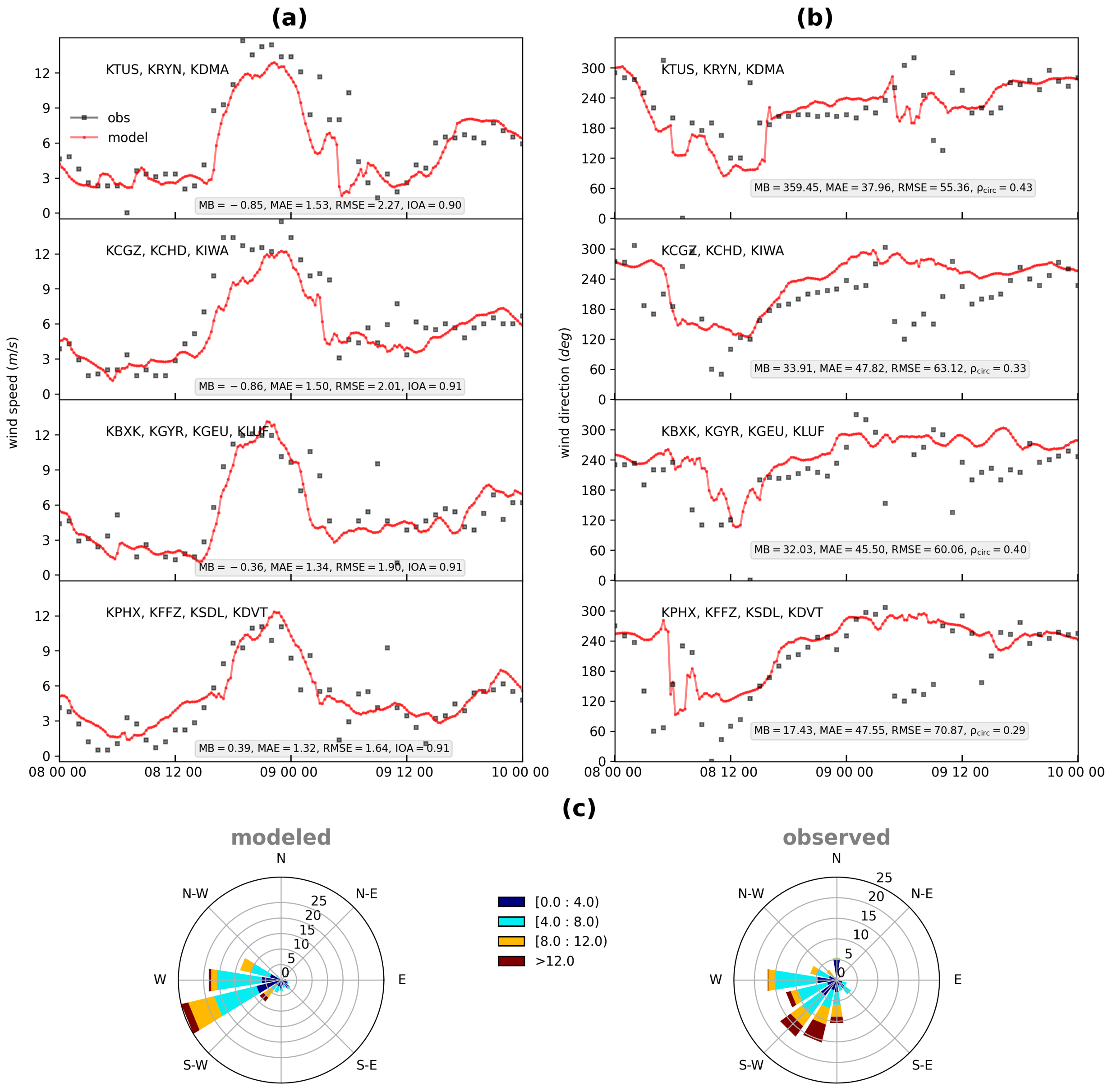

Fig. 1. Observed (black squares, hourly) and simulated (red lines, every 15 minutes) 10 m wind (a) speed and (b) direction averaged across METAR stations with names listed inset. The windroses in (c) include all the stations.

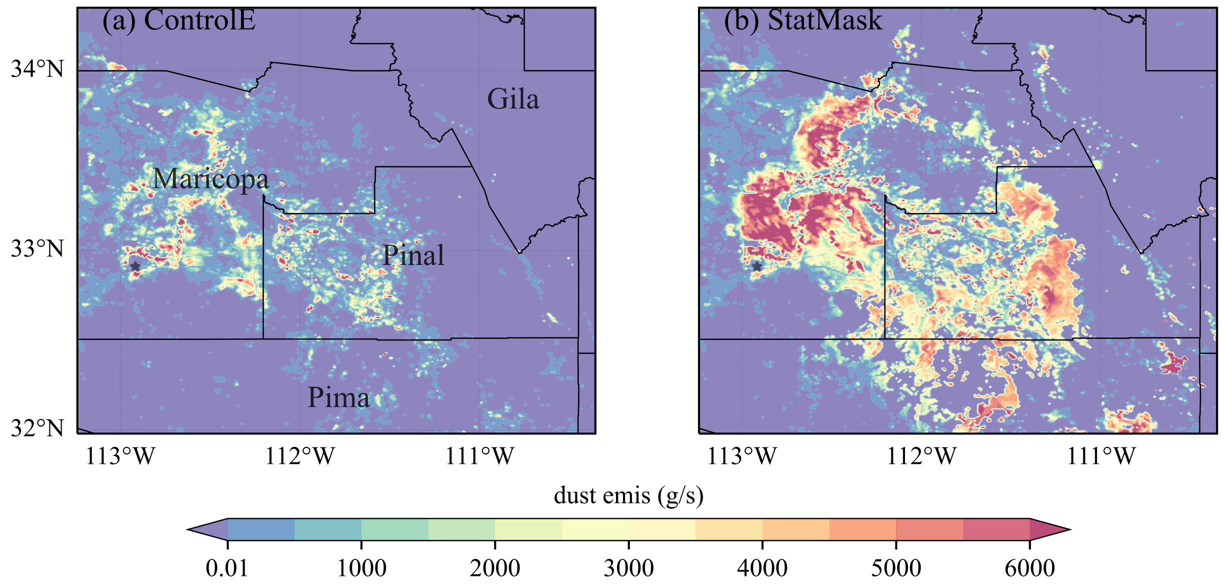

Fig. 2. Average dust emission rate (hour 21:00 on April 8) using the dynamic (a, ControlE) versus the static (b, StatMask) dust source masks. Black contours show county borders.

3.1 Sensitivity to dust source mask

Dust emissions using the two formulations for dust source mask, static (StatMask) and dynamic (ControlE), differ significantly in magnitude and spatial structure, as shown in Fig. 2. The emissions are generally stronger and more widespread in the static case. Occasionally, however, the dynamic mask emits more dust, such as at the spot just below the gray star in the figure where NDVI was so small (to have the dynamic mask value $\sim$1). The static mask also results in spurious dust emissions over some areas, such as in central Pinal or Pima counties (orange-red blobs in Fig. 2(b)), the areas not seen to be dusty in the satellite-based observations (Fig. 11(a) in J21) or in the dynamic mask (Fig. 2(a)). The lack of spatiotemporal variations, such as seasonal changes or the dynamic nature of vegetation, in the static case did not modulate dust emissions accordingly, thus allowing the emissions over areas not expected. The impact of these spurious emissions is seen in surface dust concentrations (PM_{10}) shown in Fig. 3. The difference in concentrations between the two cases is large, an order of magnitude over some areas, and is statistically significant both near the source regions and downwind (t-test, $\alpha = 0.05$; Fig. 3). A more detailed comparison, including temporal structures, is discussed next for two specific regions (chosen away from the domain boundaries to minimize the effect of any transported dust). The two regions are Phoenix (Phx) and western Pinal County (WPnl), indicated in Fig. 3.

Figure 4 shows that the static-mask simulated values (orange-red, StatMask) for both the dust variables (PM_{10} and DOD) are generally much higher than those simulated by the dynamic mask (blue, ControlE). This difference is pronounced during the peak concentration, corresponding to stronger surface winds (Fig. 1). Compared to the observation, ControlE is closer than StatMask (Fig. 4). The StatMask predictions are about 1.5–2.4 times higher than the control (Table 1). A similar factor of ~ 2 difference in dust emission and AOD was noted by an earlier study for regions with large seasonal vegetation variations (but dynamic source function producing more dust than the static; Kim et al. (2013)). The PM_{10} difference between the two simulations is larger for Phx than for WPnl, because dust emissions in StatMask are much stronger than in ControlE over areas that contributed dust to Phx (orange-red blobed areas southwest of Phx, Fig. 2(b)) compared to areas that contributed to WPnl (with winds from the southwest, Fig. 10 in J21). The agreement with observation is higher in the dynamic mask than in the static one (as indicated by larger IOA, more

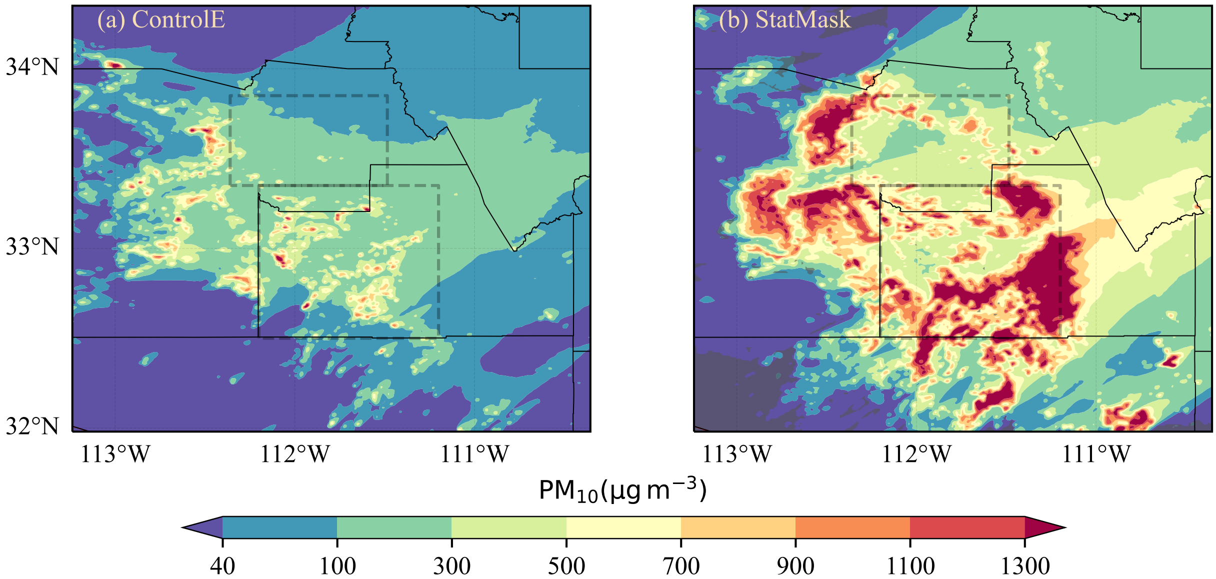

Fig. 3. PM_{10} simulated using dynamic (a, ControlE) versus static (b, StatMask) dust source masks. The difference between the two is significant (t-test, $\alpha = 0.05$) over areas excluding the overlaying dark gray shading in (b). The dashed rectangles indicate the two regions, Phoenix (Phx, upper) and western Pinal County (WPnl, lower). The values shown are an average over 30 hrs (the range shown in Fig. 4).

closer to 1 ratio of means RatM, and smaller errors MB, NMB, and MAE in Table 1). Similar conclusions follow for DOD from Table 2 that static mask overpredicted DOD compared to the dynamic one (by a factor of more than three), as well as compared to the point observation.

These results show that dust simulations using static versus dynamic dust source mask can differ significantly. Furthermore, a dynamic dust source mask, which is sensitive to changes in vegetation cover, could improve the modeling of the dust cycle as did here. A caveat to note is that the dust-emission suppression effect represented by the NDVI mask might have been less than the actual, because the NDVI mask cannot represent the effect of non-green (brown or dead) or non-photosynthetic vegetation (NPV) present over wind-erodible arid regions (Ji et al., 2017; Huang and Foroutan, 2022), including non-green crop-residue over farmlands (Tan et al., 2022). However, integrating satellite-derived NPV into dust modeling could be tricky, as the NPV corresponding to vegetation not close to the ground, such as leafless or dead standing trees, may not effectively suppress dust emission (e.g., Huang and Foroutan, 2022). Additionally, satellite-derived NPV might detect fallen leaves and litter, but strong winds could scatter this material away before the satellite observation updates (typically 1–2 times per day), making the surface beneath vulnerable to wind erosion during subsequent high winds. This wind-induced relocation, leading to a larger apparent NPV, is generally not a concern with NDVI-like indices representing green vegetation. Given no other better or more reliable options available (Okin, 2023), NDVI or similar products like leaf area index or green vegetation fraction continue to be used in dust modeling. They are expected to offer advantages over a time-static simple mask.

The difference or improvement in dust simulations with the dynamic mask is particularly expected for regions with significant seasonal or spatial vegetation-variations, such as the western US (Chapter 4 in Joshi (2023)). The difference may not be important for regions like permanent deserts with little such variations. Due to frequent changes in exposed surfaces or ground vegetation cover, cropland and rangeland are two dust sources that would particularly be represented better with a dynamic treatment for the dust source mask. The changes over cropland can occur due to agricultural activities like plowing, planting, or irrigating,

Table 1: Comparisons of PM_{10} from ControlE with each of the sensitivity experiments (StatMask, ClayKvh, FxdAdens, and Beld3Lnd), and from ControlE and each of the sensitivity experiments with the observations (Obs). The statistics (computed over the time range shown in Fig. 4) shown are: the mean bias (MB), the mean difference (MD), their absolute values (MAE and MAD, respectively), the normalized mean bias (NMB in %), the index of agreement (IOA), and the ratio of means (RatM). The suffixes 2Ctl or 2Obs indicate calculations with respect to ControlE (2Ctl) or observations (2Obs), as discussed in Sect. 2.3. Mean, MD, MAD, MB, and MAE are all in $\mu g\,m^{-3}$.

Region	Metric	ControlE	StatMask	ClayKvh	FxdAdens	Beld3Lnd	Obs
Phx	Mean	157.77	373.32	1680.73	168.95	83.49	145.4
	MD2Ctl	0.0	215.55	1522.96	11.18	-74.28	9.19
	MAD2Ctl	0.0	233.61	1522.96	11.18	74.3	79.8
	RatM2Ctl	1.0	2.37	10.65	1.07	0.53	1.06
	IOA2Ctl	1.0	0.73	0.22	1.0	0.88	0.82
	RatM2Obs	1.06	2.53	11.3	1.14	0.56	1.0
	MB2Obs	9.19	222.56	1497.64	20.1	-63.25	0.0
	NMB2Obs	6.32	153.07	1030.02	13.82	-43.5	0.0
	MAE2Obs	79.8	283.8	1519.17	87.37	80.59	0.0
	IOA2Obs	0.82	0.47	0.11	0.8	0.84	1.0
WPnl	Mean	318.56	475.65	4244.12	346.24	138.06	243.82
	MD2Ctl	0.0	157.08	3925.56	27.68	-180.5	70.36
	MAD2Ctl	0.0	166.51	3925.56	27.68	180.5	240.81
	RatM2Ctl	1.0	1.49	13.32	1.09	0.43	1.29
	IOA2Ctl	1.0	0.93	0.2	1.0	0.79	0.66
	RatM2Obs	1.29	1.92	17.16	1.4	0.56	1.0
	MB2Obs	70.36	224.13	3939.41	97.61	-106.98	0.0
	NMB2Obs	28.86	91.92	1615.71	40.03	-43.87	0.0
	MAE2Obs	240.81	363.14	3960.87	259.95	146.78	0.0
	IOA2Obs	0.66	0.51	0.06	0.62	0.77	1.0

and the changes over rangeland can occur due to seasonal or interannual variations in precipitation, as well as changes in the intensity and patterns of livestock grazing.

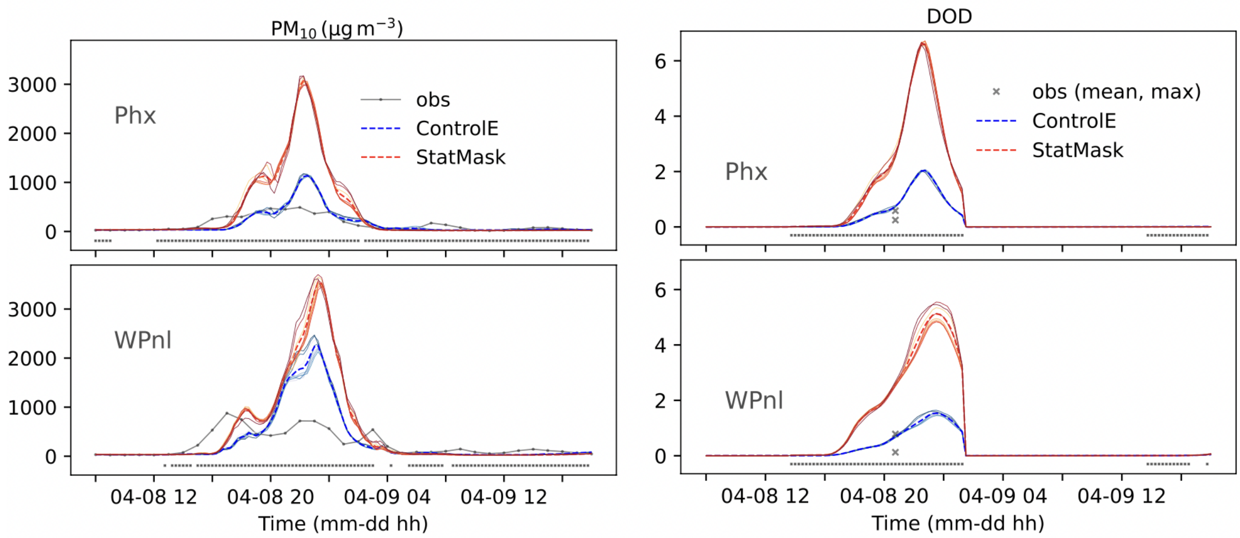

Fig. 4. (a) Average PM_{10} across the observation sites using dynamic (ControlE, blue) versus static (StatMask, orange-red) dust source masks. Thin solid lines show ensemble members and the thick dashed line shows the ensemble mean. The dotted horizontal line at the bottom indicates if the difference is significant (t-test, $\alpha = 0.05$) statistically (presence of a dot) or not (absence of a dot). The solid gray line shows observation. (b) Similar description as in (a) but for DOD. In (b) the gray crosses show the observation, as spatial mean and maximum. Phx and WPnl are the averaging regions indicated in Fig. 3.

Table 2: Similar description as in Table 1 but for DOD. InstMod and InstObs represent time-matching instantaneous values (for an instant) from model and observation, respectively.

Region	Metric	ControlE	StatMask	ClayKvh	FxdAdens	Beld3Lnd
Phx	Mean	0.21	0.69	2.47	0.23	0.12
	RatM2Ctl	1.0	3.28	11.72	1.08	0.58
	MAD2Ctl	0.0	0.48	2.26	0.02	0.09
	IOA2Ctl	1.0	0.68	0.25	1.0	0.93
	InstMod	0.74	2.62	8.15	0.8	0.46
	InstObs	0.25	0.25	0.25	0.25	0.25
WPnl	Mean	0.2	0.72	2.88	0.22	0.13
	RatM2Ctl	1.0	3.67	14.64	1.1	0.65
	MAD2Ctl	0.0	0.53	2.69	0.02	0.07
	IOA2Ctl	1.0	0.64	0.21	1.0	0.95
	InstMod	0.69	2.58	10.91	0.76	0.41
	InstObs	0.12	0.12	0.12	0.12	0.12

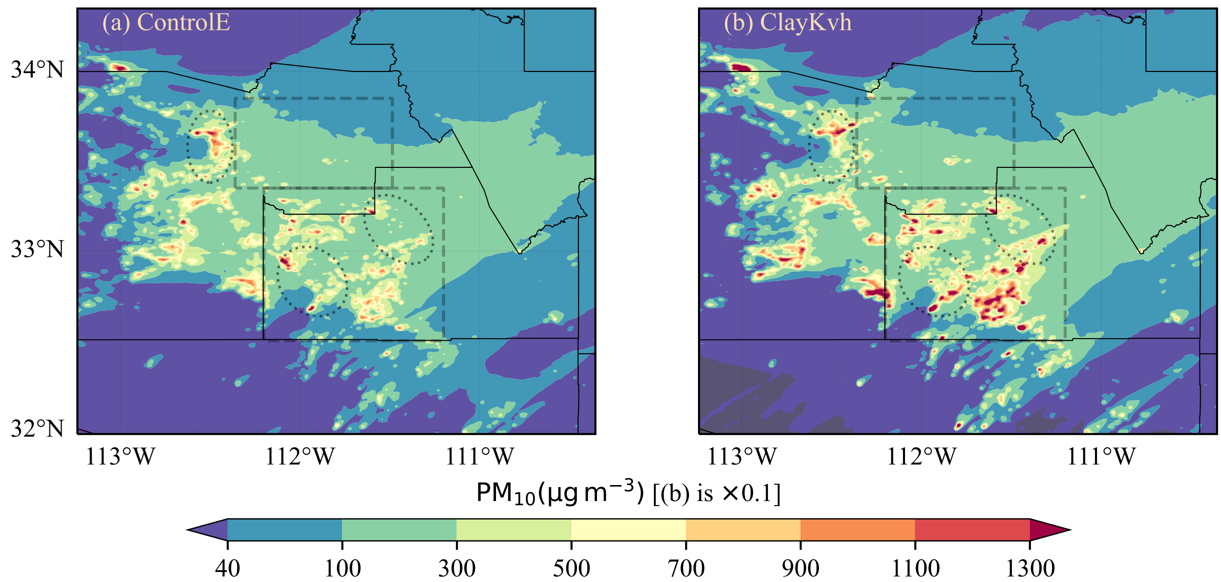

Fig. 5. Similar to Fig. 3 but using the physics-based (a, ControlE) versus the clay-based (b, ClayKvh) sandblasting efficiencies. Values in (b) are scaled by a factor of 10, as indicated over the colorbar. Dotted ellipses indicate structural nuances, like gradients, between the two cases.

3.2 Sensitivity to sandblasting efficiency

Dust modeled using the clay-based (ClayKvh) versus the physics-based (ControlE) sandblasting efficiency shows a striking difference, with the ClayKvh estimates being an order of magnitude larger than the control (Fig. 5, Fig. 6). The clay-based concentrations are $\sim$ 11 to 13 times higher than the control, and by similar measures, $\sim$ 11 to 17 times, higher than the observation (Table 1). This discrepancy exceeds 1500 $\mu\mathrm{g\,m^{-3}}$ across the observation stations in Phx, and more than twice in WPnl. The greater discrepancy in WPnl is due to proximity to dust sources. The agreement index IOA with the observation is much lower for ClayKvh (0.06–0.11) than for the control (0.66–0.82). Likewise, the errors relative to the observation are significantly larger for ClayKvh than for the control (MB, NMB, and MAE in Table 1). Column dustiness is also overestimated in ClayKvh, relative to the control (by $\sim$ 12 to 15 times) or to the observation (Table 2). The large difference between the two simulations, and over an order of magnitude discrepancy with observation in the clay-based case can be attributed to strong dependence on clay content for the ClayKvh case, in which K_{vh} can vary over a few orders of magnitude. This wide variation stems from significant clay variation over the modeling domain (Fig. 2.7 (d) in Joshi (2023)). However, there is no similar strong dependence in the

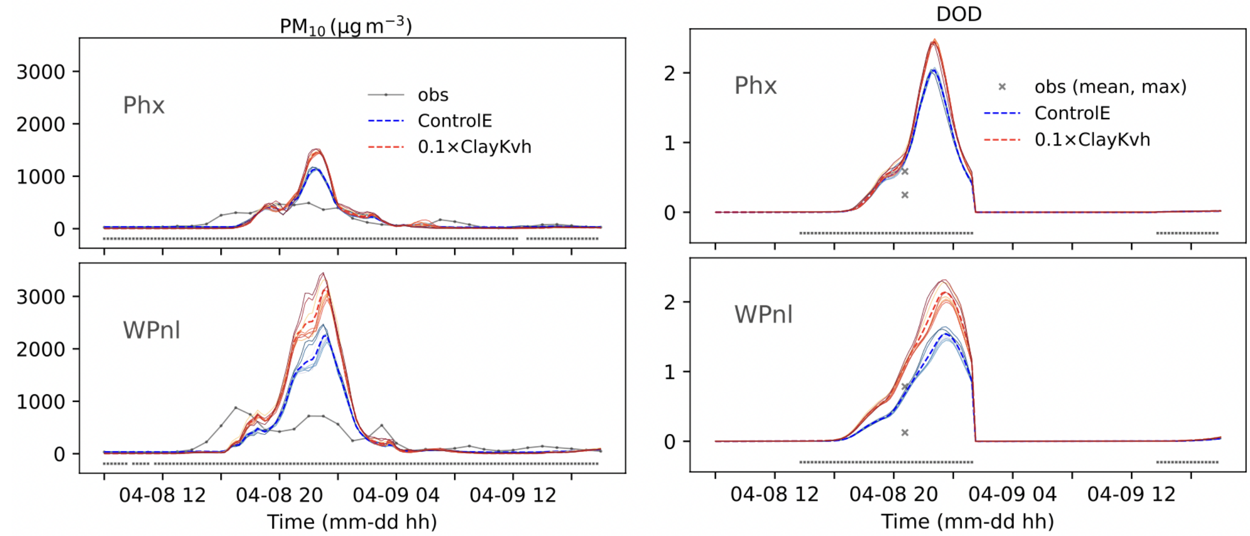

Fig. 6. Similar to Fig. 4 but using the physics-based (ControlE, blue) versus the clay-based (ClayKvh, orange-red) sandblasting efficiencies. Note the ClayKvh values are scaled (reduced) by a factor of 10.

physics-based case, in which K_{vh} variation is limited to only within a factor of around 2.

Based on these results, the clay-based versus the physics-based sandblasting efficiency could result in over an order of magnitude difference in the simulated dust. Far better agreement with observation underscores the preference for the physics-based expression, especially for regions with significant clay variation. Several other reasons also support this preference.

First, the first part of the clay-based expression in Eq. (3), derived by MB95 by fitting a simple curve to Gillette's data (Gillette, 1979), is irrelevant for soils with $clay > 0.2$. Also, this data was limited or sparse (MB95). Moreover, this expression lacks physics and can lead to serious dust overpredictions (Kang et al., 2011; Foroutan et al., 2017). MB95 cautioned about its utility, calling it a "temporary solution." Different studies have used this expression differently. Some used it as is, regardless of clay fraction exceeding 0.2 (e.g., Woodward, 2001; Hennen et al., 2023), while others assumed a uniform global clay fraction of 0.2 (Zender et al., 2003). Hennen et al. (2023) appear to have capped clay fractions above 0.2 at 0.2, leading to an implementation very similar to the ClayKvh-case here. LeGrand et al. (2023) employed it similarly and reported 'relatively small' overall effect of clay variation on dust flux, contrary to the significant effect observed in the ClayKvh-case. The author suggests an error in how the MB95 expression was implemented in LeGrand et al. (2023). Their mentioned reference LeGrand et al. (2019) notes that for clay fraction over 0–0.2 the maximum K_{vh} (their β) variation can be by only 1.08, whereas this variation should be a few orders of magnitude (see Figure 4 in MB95). With the MB95-intended implementation, the dust fluxes in LeGrand et al. (2023) would likely have varied drastically, significantly affecting the corresponding PM$_{10}$ simulations.

The second reason to prefer the physics-based expression is that the second part of Eq. (3) assumes a constant much larger than the number generally resulting from the first, effectively assuming soils with larger (generally > 0.2) clay fractions are more dust-productive. However, in the Gillette's measurements, which included soils with less than 20% clay, the lowest mean K_{vh} actually corresponded to a soil with more than 50% clay (MB95). This minimum could have occurred due to crusting of the clay-rich soil (Gillette, 1979). The physically based expression Eq. (2), however, does not imply such a constant, large value.

The limitations of the empirical relationship ($clay < 0.2$ and based on limited data) and its arbitrary use in the literature point to an urgent need for field or laboratory measurements. Such measurements would help explore or better constrain the relationship between sandblasting efficiency and globally available soil data, such as texture fractions. The arbitrary use can pose a challenge to interpreting model performances or intercomparisons.

3.3 Sensitivity to air density

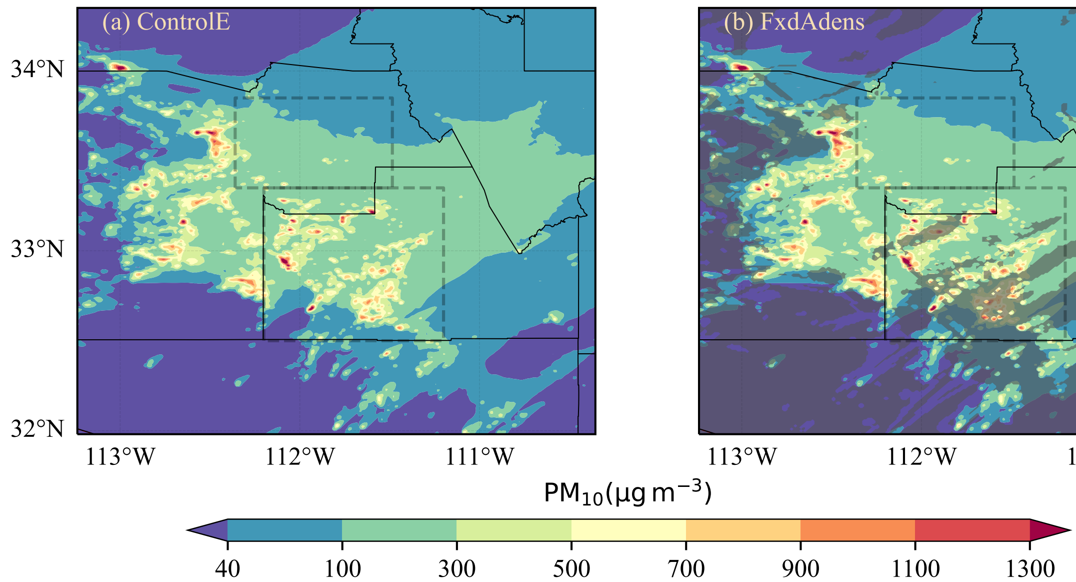

Fig. 7. Similar to Fig. 3 but using model-predicted (a, ControlE) versus a fixed constant (b, FxdAdens) for surface air density. The difference is not significant over a considerable portion of the domain, indicated by the gray shading in (b).

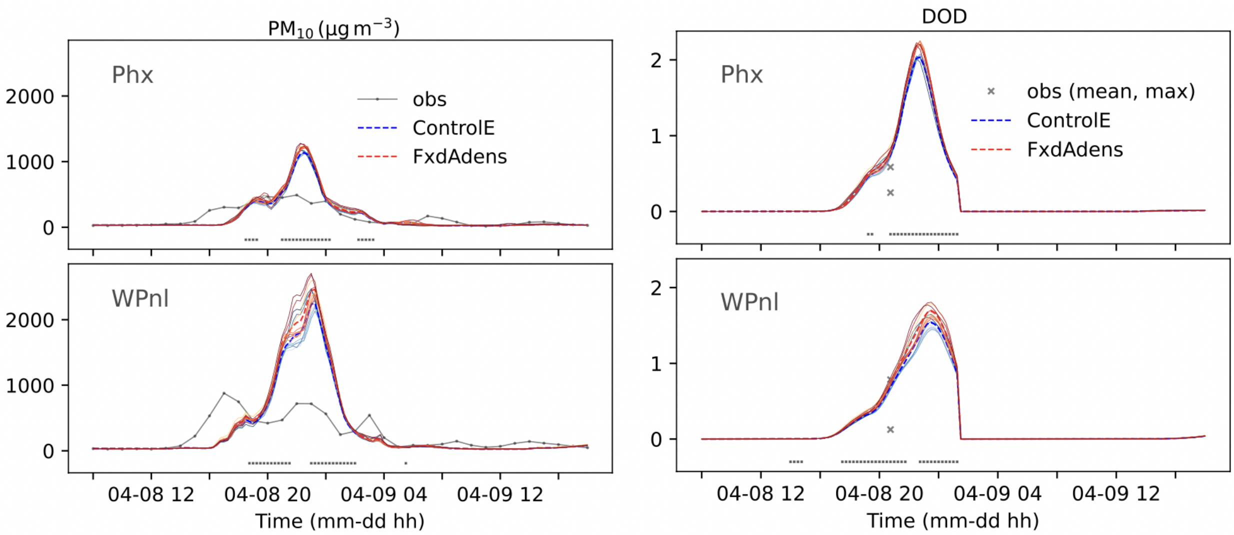

Fig. 8. Similar to Fig. 4 but using the model-predicted (ControlE, blue) versus a fixed constant (FxdAdens, orange-red) for surface air density.

The difference in dust simulations varying in air density representation is relatively small, with fixed air density (FxdAdens) resulting in slightly larger values than the model-predicted density (ControlE) (Fig. 7,

Table 1). Although small, the difference could be significant during the peak PM_{10}/DOD period (Fig. 8). The FxdAdens PM_{10} values are slightly larger than the control, by 11–28 $\mu g\,m^{-3}$or $\sim$ 8% (Table 1). The overall agreement between the two is high (IOA2Ctl $\sim$ 1). Compared to observations, ControlE appears slightly closer (with smaller errors MB, NMB, and MAE and higher IOA, Table 1). This small closeness may not represent a significant or real improvement in the control case, but it suggests that air density specification can impact dust simulations. Similar conclusions hold for DOD (Table 2).

Therefore, dust simulations using model-predicted versus a fixed constant for air density can differ by a non-negligible margin. The difference would be much larger for longer simulations including seasonal changes (Fig. S1(c) and Fig. S2 in the Supplementary material). Consequently, the model-predicted option is preferable to account for realistic density variations, particularly in regions with significant diurnal or seasonal cycles and elevation differences. The increase in compute time in this study for the model-predicted option compared to the fixed constant was imperceptible.

3.4 Sensitivity to land use

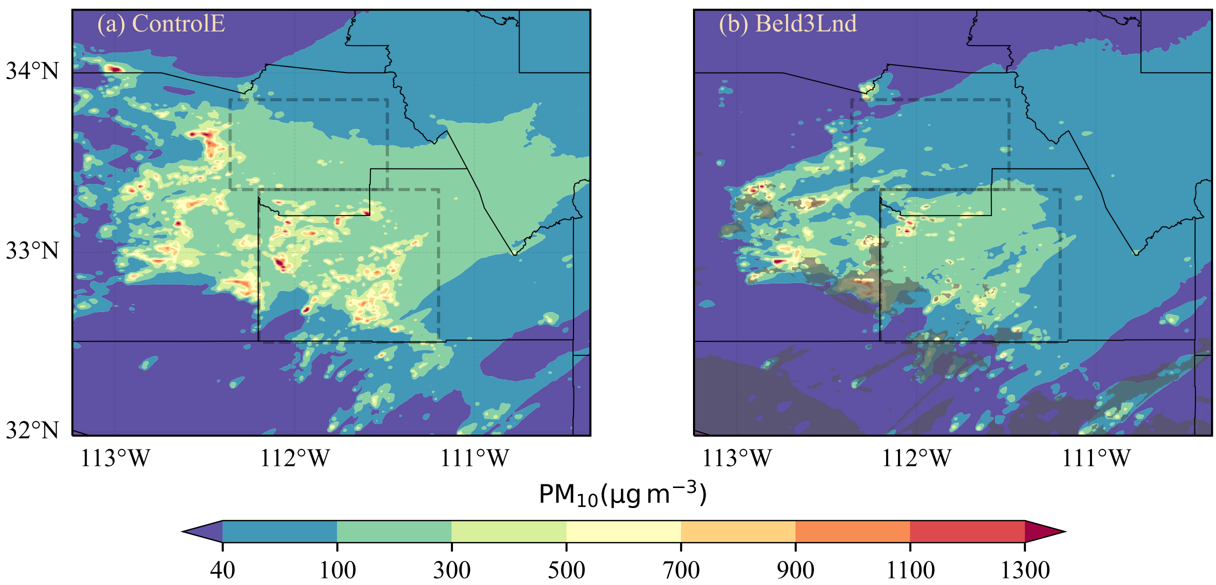

Fig. 9. Similar to Fig. 3 but using the up-to-date (a, ControlE) versus the old (b, Beld3Lnd) land use data.

Dust simulations with the old (Beld3Lnd) and up-to-date (ControlE) data for land use differ significantly in magnitude and structure (Fig. 9, Fig. 10). Modeled dust is generally smaller in the old data due to smaller cropland or greater shrubland fraction over the dust-producing region. This is expected as shrubland requires stronger winds to emit dust compared to cropland. For this reason, in Fig. 9 the dust plumes over the northwestern part of the domain and the wide, high-concentration plume extending to the southern Gila county from the WPnl region in the control case are both missing in Beld3Lnd. Furthermore, the sensitivity to land use is greater in WPnl than in Phx, as can be seen from the difference in the gaps between the blue and the orange-red PM_{10} curves in Fig. 10. The higher sensitivity in WPnl is due to the proximity of the averaging locations to the stronger emission sources (Fig. 9).

At the start and the end of the peak concentration period in Fig. 10, Beld3Lnd highly underpredicted concentrations, while ControlE indicated dust activity (high PM_{10}) more consistent with observation. Overall, the Beld3Lnd values are smaller than the control by $\sim$ 74–180 $\mu g\,m^{-3}$ or a factor of around 2 (RatM2Ctl 0.43–0.53; Table 1). Compared to observations, Beld3Lnd underpredicted the concentrations by a factor of around 2 in Phx (RatM2Obs 0.56), whereas ControlE predicted them well (RatM2Obs near 1.0). ControlE generally aligns better with observations, except during the peak when Beld3Lnd performs better (Fig. 10). This contrasting behavior during the peak period is due to ControlE significantly overpredicting the peak values, particularly in WPnl (Fig. 10). This is reflected as both experiments having similar absolute error MAE for Phx but differing for WPnl, where ControlE exhibits a larger error (Table 1). The pronounced overprediction during the peak, compared to observations, could be attributed to biases in the simulated meteorology (Sect. 3.0.1). Addressing these biases would likely bring ControlE closer to observations, while causing Beld3Lnd to deviate further, shifting the Beld3Lnd curve downward (Fig. 10). This meteorology-induced effect is likely because a meteorological nudging brings the ControlE PM_{10} values, particularly around the peak, to lower levels, closer to observations (Fig. 3.14 in Joshi (2023)).

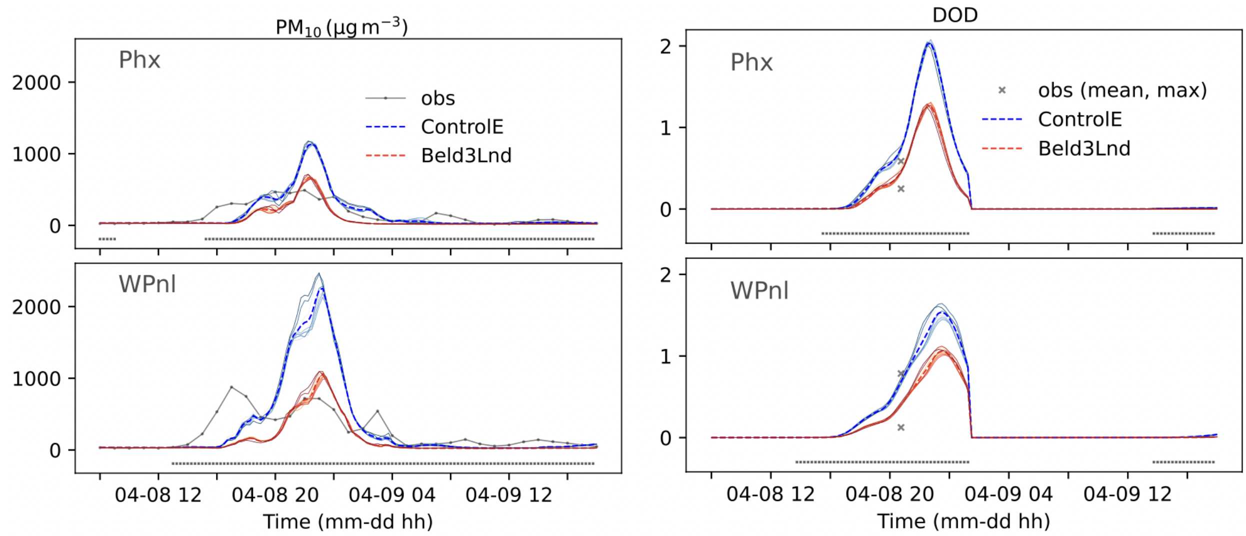

Fig. 10. Similar to Fig. 4 but using the up-to-date (ControlE, blue) versus the old (Beld3Lnd, orange-red) land use data.

These results show that dust simulations could be sensitive to land use or land use data (old versus new) and could be improved significantly using more accurate data. The actual sensitivity is likely greater than the one estimated because the dust source mask remained the same, corresponding to ControlE or up-to-date land use data, which includes a higher proportion of cropland (a relatively more erodible land type). Isolating the land use effect further should be the subject of future studies.

The significant sensitivity underscores the influence of land use changes in central Arizona on regional dust emission. The land use change in this case doubled the dust emission, implying potential impacts of future land use changes on the region's dust activity. Therefore, updating land use data, often overlooked in models, is crucial for dust or air quality modeling because land use might have changed (or will change), as it has for Phoenix and the surrounding areas (e.g., Jenerette and Wu, 2001), in response to environmental or climatic conditions or socio-economic factors, including migration, infrastructure development, and agricultural activities or expansions (Lark et al., 2015; Lambert et al., 2020). In the western US dust-source regions, factors such as water availability, highway construction, and city expansion have led to conversions from agricultural lands to abandoned, desert, or urban and builtup areas (Hyers and Marcus, 1981; Baxter and Calvert, 2017), or from uncultivated lands to cultivated ones (Lark et al., 2015). Such conversions can impact regional dust activity, as wind erosion depends on land use or land cover (Gillette et al., 1978; Joshi, 2021).

3.5 Uncertainty due to meteorology

An additional experiment was carried out by enabling meteorological nudging (observation and analysis), but otherwise leaving the configuration identical to ControlE. Dust simulation ratios of means to control for this experiment were 1.01 and 0.71 for PM_{10} (and 0.88 and 0.61 for DOD) for Phx and WPnl, respectively. Dust concentrations could therefore differ by nearly 30% solely due to uncertainty in meteorology. However, these ratios are generally much closer to unity than for the parameter sensitivities discussed above. Thus, the differences in dust simulations for each pair of experiments involving dust source mask, sandblasting efficiency, and land use data are robust to meteorological variations. The difference for air density, however, is comparable to or within the meteorological uncertainty. Future studies should explore more the role of meteorological uncertainty, including *sensitive dependence on initial conditions* or atmospheric *chaos* toward which some effort is underway (Joshi and Shukla, 2023).

3.6 Implications for dust modeling in general

The sensitivity analysis presented above, while specific to a particular dust emission scheme, is relevant for many other dust emission schemes in general, which typically use a similar flux equation (as Eq. (1)). In these schemes, the four parameters generally affect the flux in similar ways, and therefore, a comparable level of model sensitivity could be expected. One key difference to note however is that in other dust schemes, the input air density (ρ_a) also impacts the threshold friction velocity u_{*t}, unlike in the scheme used above. To the author's knowledge, the sensitivity to air density has rarely been studied. Specifically, Darmenova et al. (2009) reported air density sensitivity of u_{*t}, corresponding to average air density over three Asian dust regions. The present study goes further and provides uncertainty in dust fluxes. Furthermore, the analysis here includes a whole year to account for seasonal changes and incorporates global dust source regions.

The fractional uncertainty in dust flux (F) is computed as $\frac{\Delta F}{F} = \frac{f(\rho_{a,0}) - f(\rho_{a,ex})}{f(\rho_{a,ex})} \times 100\%$, where f is the part of the dust flux expression that depends on input air density (ρ_a), $\rho_{a,ex}$ is the expected or actual air density, and $\rho_{a,0} = 1.23\,\mathrm{kg\,m^{-3}}$ is the commonly used constant for air density. Three cases of dust emission schemes are considered: first, the scheme as used in this study (Eq. (1)) for which $f = \rho_a$; second, similar to the first (Owen, 1964; Shao et al., 1996), but $f = \rho_a u_* (u_*^2 - [u_{*t}(\rho_a)]^2)$, where $u_{*t}(\rho_a)$ indicates ρ_a dependence of u_{*t}; and third, the scheme of Marticorena and Bergametti (1995) or MB95 for which $f = \rho_a (u_* + [u_{*t}(\rho_a)])(u_*^2 - [u_{*t}(\rho_a)]^2)$. For simplicity, $u_* = 1\,\mathrm{m\,s^{-1}}$ is assumed. The $u_{*t}(\rho_a)$ is calculated using the parameterization of MB95 for a saltating particle of diameter 75 μm (which yields $\sim 0.20\,\mathrm{m\,s^{-1}}$ for $\rho_a = \rho_{a,0}$). The u_{*t} has an inverse relation with ρ_a.

The annual variation in air density over most of the arid regions ranges between 10–22% and is maximum over Asian deserts such as Taklimakan and Gobi, and relatively less over lower-latitude arid regions in both the hemispheres, including the modeling domain of this study where the variation is around 15% (Fig. S1(b,c) in the Supplementary material). Dust flux variations for the first case of the emission schemes would be similar in magnitude to these density variations. The fractional uncertainty in dust flux for the first case ranges from 8 to 20% over most of the dust source regions, corresponding to the minimum expected air density (Fig. S2). The uncertainty increases slightly for the second case (Fig. S3) as expected, because of the additional uncertainty from the u_{*t} term. For the third case, the uncertainty decreases from the second and is similar to or slightly less than in the first. The decrease in this case can be attributed to the opposing contributions from the terms $(u_* + u_{*t})$ and $(u_*^2 - [u_{*t}(\rho_a)]^2)$. Thus, it may be concluded that the uncertainty in dust flux due to air density representation is dominantly through the ρ_a term explicitly appearing in the flux equations.

Given the significant uncertainty that can arise from fixing air density to a constant, the model-predicted option is recommended, particularly for ρ_a explicitly occurring in the flux equation. For u_{*t}, an appropriate constant for air density may suffice (Fig. S1(a)) if the computing time becomes a concern, as u_{*t} changes only by $\sim$ 0.04 $\mathrm{ms^{-1}}$ for density over a wide range, 0.9–1.26 $\mathrm{kg\,m^{-3}}$. Although the uncertainty is the least corresponding to the maximum air density (Fig. S2–4), more relevant for practical considerations is the uncertainty corresponding to the minimum air density (when the uncertainty is the greatest). This is because dust storms tend to occur in the afternoon hours between 12:00 and 20:00 LST, or during periods of maximum thermal instability (Orgill and Sehmel, 1976; Mbourou et al., 1997) when the air density tends to be minimal (Fig. S1(c)). Thus, the commonly used 1.23 $\mathrm{kg\,m^{-3}}$ for air density appears to be an overestimate and not optimal for most dust source regions (Fig. S1).

4. Conclusions

This study quantified dust simulation uncertainties associated with representations for four important parameters in a dust emission model. The results reveal significant differences in dust concentration and optical depth: twofold between static and dynamic dust source masks, tenfold between clay-based and physics-based sandblasting efficiencies, and twofold between old and up-to-date land use data. These parameter sensitivities surpass meteorology-induced uncertainty and support conclusions consistent with physical reasoning—simulations better match observation when using a dynamic dust source mask, a physics-based sandblasting efficiency, and up-to-date land use data. Sensitivity to surface air density is small and comparable to meteorological uncertainty but would be larger for longer simulations. For major global dust source regions, up to 22% uncertainty in dust flux can occur when ignoring air density variations. Although the literature acknowledges the potential impacts of these parameter representations, at least qualitatively, a detailed quantitative analysis appears to be lacking. Moreover, studies often neglect updating land use data or dust source mask and ignore the effect of air density variation, in addition to implementing arbitrarily the empirical relation for sandblasting efficiency. Failing to consider these parameter uncertainties could mislead model development and could lead to incorrect interpretations of model-observation discrepancies. The significant sensitivities identified and discussed in this study therefore have implications for improving the dust cycle in weather and climate models and interpreting intermodel differences.

Notably, parameter sensitivity could be season-dependent, influenced by whether a dust event is frontal or convective, or by seasonal vegetation dynamics affecting the dust source mask. It could be region-dependent as well, due to spatial variations in clay content or erodible land types. More work is needed to isolate the effect of land use data, which is likely underestimated. Future studies should explore or test other options for dust source mask (including the effect of non-green vegetation) and sandblasting efficiency. To better constrain the 'sandblasting efficiency-soil property' empirical relationship, additional measurements are urgently needed. Model development will also need to investigate sensitivity to size distribution, deposition scheme, and threshold friction velocity. The albedo-based drag-partitioning used in recent studies could have much less process fidelity than claimed (Okin, 2023). Further research is required to explore the range of uncertainty caused by meteorology for which some effort is underway.

Data availability

The research data from this study are available upon request. The ERA5-Land data was downloaded from `https://cds.climate.copernicus.eu` (DOI: 10.24381/cds.e2161bac, Accessed 23-Apr-2024). Other data sources can be found in the open-access article Joshi (2021).

Funding

This research did not receive any specific grant from funding agencies in the public, commercial, or not-for-profit sectors.

Acknowledgments

I express my gratitude to George Mason University (GMU) College of Science for the graduate research assistantship support during my Ph.D. and to the GMU Office of Research Computing for computing resources. I would like to thank my doctoral advisor and Distinguished University Professor, Dr. Jagadish Shukla, for useful suggestions and comments on a very early version of the manuscript. I also thank Dr. Daniel Tong for facilitating/providing access to computing resources and data storage and for comments on a very early version. I acknowledge the providers of the data used. My sincere thanks extend to the editor and anonymous reviewers for insightful suggestions that improved this paper.

References

Alfaro, S.C., Gomes, L., 2001. Modeling mineral aerosol production by wind erosion: Emission intensities and aerosol size distributions in source areas. Journal of Geophysical Research: Atmospheres 106, 18075–18084. https://doi.org/10.1029%2F2000jd900339.

Bagnold, R.A., 1941. The Physics of Blown Sand and Desert Dunes. London: Methuen. https://doi.org/10.1007%2F978-94-009-5682-7.

Baxter, R.E., Calvert, K.E., 2017. Estimating available abandoned cropland in the United States: Possibilities for energy crop production. Annals of the American Association of Geographers 107, 1162–1178. https://doi.org/10.1080/24694452.2017.1298985.

Colarco, P., Toon, O., Holben, B., 2003. Saharan dust transport to the Caribbean during PRIDE: 1. Influence of dust sources and removal mechanisms on the timing and magnitude of downwind aerosol optical depth events from simulations of in situ and remote sensing observations. Journal of Geophysical Research: Atmospheres 108. https://doi.org/10.1029/2002JD002658.

d'Almeida, G.A., 1987. On the variability of desert aerosol radiative characteristics. Journal of Geophysical Research: Atmospheres 92, 3017–3026. https://doi.org/10.1029/JD092iD03p03017.

Darmenova, K., Sokolik, I.N., Shao, Y., Marticorena, B., Bergametti, G., 2009. Development of a physically based dust emission module within the Weather Research and Forecasting (WRF) model: Assessment of dust emission parameterizations and input parameters for source regions in Central and East Asia. J. Geophys. Res. 114. https://doi.org/10.1029%2F2008jd011236.

Dong, X., Fu, J.S., Huang, K., Tong, D., Zhuang, G., 2016. Model development of dust emission and heterogeneous chemistry within the Community Multiscale Air Quality modeling system and its application over East Asia. Atmos. Chem. Phys. 16, 8157–8180. https://doi.org/10.5194%2Facp-16-8157-2016.

Fécan, F., Marticorena, B., Bergametti, G., 1999. Parametrization of the increase of the aeolian erosion threshold wind friction velocity due to soil moisture for arid and semi-arid areas. Annales Geophysicae 17, 149. https://doi.org/10.1007%2Fs005850050744.

Foroutan, H., Young, J., Napelenok, S., Ran, L., Appel, K.W., Gilliam, R.C., Pleim, J.E., 2017. Development and evaluation of a physics-based windblown dust emission scheme implemented in the CMAQ modeling system. J. Adv. Model. Earth Syst. 9, 585–608. https://doi.org/10.1002%2F2016ms000823.

Fu, X., Wang, S., Cheng, Z., Xing, J., Zhao, B., Wang, J., Hao, J., 2014. Source, transport and impacts of a heavy dust event in the Yangtze River Delta, China, in 2011. Atmospheric Chemistry and Physics 14, 1239–1254. https://doi.org/10.5194%2Facp-14-1239-2014.

Gillette, D., 1979. Environmental factors affecting dust emission by wind erosion. Saharan dust. Edited by C. Morales, pp 71–94, John Wiley, New York.

Gillette, D., Clayton, R., Mayeda, T., Jackson, M., Sridhar, K., 1978. Tropospheric aerosols from some major dust storms of the southwestern United States. J. Appl. Meteor. Climatol. 17, 832–845. https://doi.org/10.1175/1520-0450(1978)017<0832:TAFSMD>2.0.CO;2.

Gillette, D.A., Passi, R., 1988. Modeling dust emission caused by wind erosion. Journal of Geophysical Research: Atmospheres 93, 14233–14242. https://doi.org/10.1029/JD093iD11p14233.

Ginoux, P., Chin, M., Tegen, I., Prospero, J.M., Holben, B., Dubovik, O., Lin, S.J., 2001. Sources and distributions of dust aerosols simulated with the GOCART model. Journal of Geophysical Research: Atmospheres 106, 20255–20273. https://doi.org/10.1029%2F2000jd000053.

Ginoux, P., Prospero, J.M., Gill, T.E., Hsu, N.C., Zhao, M., 2012. Global-scale attribution of anthropogenic and natural dust sources and their emission rates based on MODIS Deep Blue aerosol products. Rev. Geophys. 50. https://doi.org/10.1029%2F2012rg000388.

Grini, A., Zender, C.S., 2004. Roles of saltation, sandblasting, and wind speed variability on mineral dust aerosol size distribution during the Puerto Rican Dust Experiment (PRIDE). Journal of Geophysical Research: Atmospheres 109. https://doi.org/10.1029/2003JD004233.

Han, W., Yang, Z., Di, L., Mueller, R., 2012. CropScape: A web service based application for exploring and disseminating US conterminous geospatial cropland data products for decision support. Computers and Electronics in Agriculture 84, 111–123. https://doi.org/10.1016%2Fj.compag.2012.03.005.

Hennen, M., Chappell, A., Webb, N.P., 2023. Modelled direct causes of dust emission change (2001–2020) in southwestern USA and implications for management. Aeolian Research 60, 100852. https://doi.org/10.1016/j.aeolia.2022.100852.

Huang, X., Foroutan, H., 2022. Effects of non-photosynthetic vegetation on dust emissions. Journal of Geophysical Research: Atmospheres 127, e2021JD035243. https://doi.org/10.1029/2021JD035243.

Huneeus, N., Schulz, M., Balkanski, Y., Griesfeller, J., Prospero, J., Kinne, S., Bauer, S., Boucher, O., Chin, M., Dentener, F., Diehl, T., Easter, R., Fillmore, D., Ghan, S., Ginoux, P., Grini, A., Horowitz, L., Koch, D., Krol, M.C., Landing, W., Liu, X., Mahowald, N., Miller, R., Morcrette, J.J., Myhre, G., Penner, J., Perlwitz, J., Stier, P., Takemura, T., Zender, C.S., 2011. Global dust model intercomparison in AeroCom phase I. Atmos. Chem. Phys. 11, 7781–7816. https://doi.org/10.5194%2Facp-11-7781-2011.

Hyers, A.D., Marcus, M., 1981. Land use and desert dust hazards in central Arizona. Geol. Soc. Am. Spec. Pap 186, 267–280. https://doi.org/10.1130%2Fspe186-p267.

Jenerette, G.D., Wu, J., 2001. Analysis and simulation of land-use change in the central Arizona–Phoenix region, USA. Landscape ecology 16, 611–626. https://doi.org/10.1023/A:1013170528551.

Ji, C., Jia, Y., Gao, Z., Wei, H., Li, X., 2017. Nonlinear spectral mixture effects for photosynthetic/non-photosynthetic vegetation cover estimates of typical desert vegetation in western China. Plos one 12, e0189292. https://doi.org/10.1371/journal.pone.0189292.

Joshi, J., Shukla, J., 2023. "Butterfly Effect" for Dust Storms, in: AGU Fall Meeting Abstracts, pp. A31J–2526.

Joshi, J.R., 2021. Quantifying the impact of cropland wind erosion on air quality: A high-resolution modeling case study of an Arizona dust storm. Atmospheric Environment 263, 118658. https://doi.org/10.1016/j.atmosenv.2021.118658.

Joshi, J.R., 2023. Modeling and Predictability of Dust Storms and Atmospheric Dustiness Over the Western United States. Ph.D. thesis. George Mason University. ISBN 9798379706241, Publicatin No. 30425455.

Kang, J.Y., Yoon, S.C., Shao, Y., Kim, S.W., 2011. Comparison of vertical dust flux by implementing three dust emission schemes in WRF/Chem. J. Geophys. Res. 116. https://doi.org/10.1029%2F2010jd014649.

Kim, D., Chin, M., Bian, H., Tan, Q., Brown, M.E., Zheng, T., You, R., Diehl, T., Ginoux, P., Kucsera, T., 2013. The effect of the dynamic surface bareness on dust source function, emission, and distribution. Journal of Geophysical Research: Atmospheres 118, 871–886. https://doi.org/10.1029/2012JD017907.

Kinnee, E., Geron, C., Pierce, T., 1997. United States land use inventory for estimating biogenic ozone precursor emissions. Ecological Applications 7, 46–58. https://doi.org/10.1890/1051-0761(1997)007[0046:USLUIF]2.0.CO;2.

Kok, J., Mahowald, N., Fratini, G., Gillies, J., Ishizuka, M., Leys, J., Mikami, M., Park, M.S., Park, S.U., Van Pelt, R., et al., 2014. An improved dust emission model–part 1: Model description and comparison against measurements. Atmospheric Chemistry and Physics 14, 13023–13041. https://doi.org/10.5194/acp-14-13023-2014.

Kok, J.F., 2011. A scaling theory for the size distribution of emitted dust aerosols suggests climate models underestimate the size of the global dust cycle. Proceedings of the National Academy of Sciences 108, 1016–1021. https://doi.org/10.1073/pnas.1014798108.

Lambert, A., Hallar, A.G., Garcia, M., Strong, C., Andrews, E., Hand, J.L., 2020. Dust impacts of rapid agricultural expansion on the great plains. Geophysical Research Letters 47, e2020GL090347. https://doi.org/10.1029/2020GL090347.

Lark, T.J., Salmon, J.M., Gibbs, H.K., 2015. Cropland expansion outpaces agricultural and biofuel policies in the United States. Environmental Research Letters 10, 044003. https://doi.org/10.1088/1748-9326/10/4/044003.

LeGrand, S.L., Letcher, T.W., Okin, G.S., Webb, N.P., Gallagher, A.R., Dhital, S., Hodgdon, T.S., Ziegler, N.P., Michaels, M.L., 2023. Application of a satellite-retrieved sheltering parameterization (v1. 0) for dust event simulation with WRF-Chem v4. 1. Geoscientific Model Development 16, 1009–1038. https://doi.org/10.5194/gmd-16-1009-2023.

Liang, Y., Wu, C., Ji, X., Zhang, M., Li, Y., He, J., Qin, Z., 2022. Estimation of the influences of spatiotemporal variations in air density on wind energy assessment in china based on deep neural network. Energy 239, 122210. https://doi.org/10.1016/j.energy.2021.122210.

Lu, H., Shao, Y., 1999. A new model for dust emission by saltation bombardment. J. Geophys. Res.: Atmos. 104, 16827–16842. https://doi.org/10.1029%2F1999jd900169.

Maring, H., Savoie, D., Izaguirre, M., Custals, L., Reid, J., 2003. Mineral dust aerosol size distribution change during atmospheric transport. Journal of Geophysical Research: Atmospheres 108. https://doi.org/10.1029/2002JD002536.

Marticorena, B., Bergametti, G., 1995. Modeling the atmospheric dust cycle: 1. Design of a soil-derived dust emission scheme. J. Geophys. Res. 100, 16415. https://doi.org/10.1029%2F95jd00690.

Mbourou, G., Bertrand, J., Nicholson, S., 1997. The diurnal and seasonal cycles of wind-borne dust over Africa north of the equator. Journal of Applied Meteorology and Climatology 36, 868–882. https://doi.org/10.1175/1520-0450(1997)036<0868:TDASCO>2.0.CO;2.

Menut, L., Foret, G., Bergametti, G., 2007. Sensitivity of mineral dust concentrations to the model size distribution accuracy. Journal of Geophysical Research: Atmospheres 112. https://doi.org/10.1029/2006JD007766.

Menut, L., Pérez, C., Haustein, K., Bessagnet, B., Prigent, C., Alfaro, S., 2013. Impact of surface roughness and soil texture on mineral dust emission fluxes modeling. Journal of Geophysical Research: Atmospheres 118, 6505–6520. https://doi.org/10.1002/jgrd.50313.

Muñoz-Sabater, J. et al., 2021. ERA5-Land: a state-of-the-art global reanalysis dataset for land applications. Earth Syst. Sci. Data 13, 4349–4383. DOI: 10.24381/cds.68d2bb30 (Accessed 23-Apr-2024).

Nowottnick, E., Colarco, P., da Silva, A., Hlavka, D., McGill, M., 2011. The fate of saharan dust across the atlantic and implications for a central american dust barrier. Atmospheric Chemistry and Physics 11, 8415–8431. https://doi.org/10.5194/acp-11-8415-2011.

Okin, G.S., 2023. Shadow is related to roughness but modis brdf should not be used to estimate lateral cover. Remote Sensing of Environment 292, 113581. https://doi.org/10.1016/j.rse.2023.113581.

Orgill, M., Sehmel, G., 1976. Frequency and diurnal variation of dust storms in the contiguous USA. Atmospheric Environment (1967) 10, 813–825. https://doi.org/10.1016/0004-6981(76)90136-0.

Owen, P.R., 1964. Saltation of uniform grains in air. J. Fluid Mech. 20, 225–242. https://doi.org/10.1017%2Fs0022112064001173.

Prospero, J.M., Ginoux, P., Torres, O., Nicholson, S.E., Gill, T.E., 2002. Environmental characterization of global sources of atmospheric soil dust identified with the Nimbus 7 Total Ozone Mapping Spectrometer (TOMS) absorbing aerosol product. Reviews of geophysics 40, 2–1. https://doi.org/10.1029/2000RG000095.

Raupach, M.R., Lu, H., 2004. Representation of land-surface processes in aeolian transport models. Environmental Modelling & Software 19, 93–112. https://doi.org/10.1016/S1364-8152(03)00113-0.

Schulz, M., Balkanski, Y.J., Guelle, W., Dulac, F., 1998. Role of aerosol size distribution and source location in a three-dimensional simulation of a Saharan dust episode tested against satellite-derived optical thickness. Journal of Geophysical Research: Atmospheres 103, 10579–10592. https://doi.org/10.1029/97JD02779.

Shao, Y., 2008. Physics and modelling of wind erosion. Springer. https://doi.org/10.1007/978-1-4020-8895-7.

Shao, Y., Ishizuka, M., Mikami, M., Leys, J., 2011. Parameterization of size-resolved dust emission and validation with measurements. Journal of Geophysical Research: Atmospheres 116. https://doi.org/10.1029/2010JD014527.

Shao, Y., Raupach, M., Leys, J., 1996. A model for predicting aeolian sand drift and dust entrainment on scales from paddock to region. Soil Res. 34, 309. https://doi.org/10.1071%2Fsr9960309.

Shao, Y., Raupach, M.R., Findlater, P.A., 1993. Effect of saltation bombardment on the entrainment of dust by wind. J. Geophys. Res. 98, 12719. https://doi.org/10.1029%2F93jd00396.

Tan, J., Wu, X., Zeng, F., Li, X., Feng, M., Liao, G., Sha, R., 2022. Effects of crop residue on wind erosion due to dust storms in Hotan Prefecture, Xinjiang, China. Soil and Tillage Research 221, 105387. https://doi.org/10.1016/j.still.2022.105387.

Tegen, I., Fung, I., 1994. Modeling of mineral dust in the atmosphere: Sources, transport, and optical thickness. Journal of Geophysical Research: Atmospheres 99, 22897–22914. https://doi.org/10.1029/94JD01928.

Timmreck, C., Schulz, M., 2004. Significant dust simulation differences in nudged and climatological operation mode of the AGCM ECHAM. Journal of Geophysical Research: Atmospheres 109. https://doi.org/10.1029/2003JD004381.

Todd, M.C., Karam, D.B., Cavazos, C., Bouet, C., Heinold, B., Baldasano, J.M., Cautenet, G., Koren, I., Perez, C., Solmon, F., Tegen, I., Tulet, P., Washington, R., Zakey, A., 2008. Quantifying uncertainty in estimates of mineral dust flux: An intercomparison of model performance over the Bodélé Depression, northern Chad. J. Geophys. Res. 113. https://doi.org/10.1029%2F2008jd010476.

Uno, I., Wang, Z., Chiba, M., Chun, Y., Gong, S.L., Hara, Y., Jung, E., Lee, S.S., Liu, M., Mikami, M., et al., 2006. Dust model intercomparison (DMIP) study over Asia: Overview. Journal of Geophysical Research: Atmospheres 111. https://doi.org/10.1029/2005JD006575.

Webb, N.P., Strong, C.L., 2011. Soil erodibility dynamics and its representation for wind erosion and dust emission models. Aeolian Research 3, 165–179. https://doi.org/10.1016/j.aeolia.2011.03.002.

White, B.R., 1979. Soil transport by winds on Mars. Journal of Geophysical Research: Solid Earth 84, 4643–4651. https://doi.org/10.1029/JB084iB09p04643.

Woodward, S., 2001. Modeling the atmospheric life cycle and radiative impact of mineral dust in the Hadley Centre climate model. Journal of Geophysical Research: Atmospheres 106, 18155–18166. https://doi.org/10.1029/2000JD900795.

Wu, C., Lin, Z., Liu, X., 2020. The global dust cycle and uncertainty in CMIP5 (Coupled Model Intercomparison Project phase 5) models. Atmospheric Chemistry and Physics 20, 10401–10425. https://doi.org/10.5194/acp-20-10401-2020.

Zender, C.S., Bian, H., Newman, D., 2003. Mineral Dust Entrainment and Deposition (DEAD) model: Description and 1990s dust climatology. Journal of Geophysical Research: Atmospheres 108. https://doi.org/10.1029/2002JD002775.